Facies (2021) 67:18
https://doi.org/10.1007/s10347-021-00626-z

ORIGINAL ARTICLE

Facies analysis of the Upper Ordovician Xiazhen Formation, southeast China: Implications for carbonate platform development in South China prior to the onset of the Hirnantian glaciation

Jino Park[1,2] · Jeong-Hyun Lee[3] · Kun Liang[4] · Suk-Joo Choh[5]

Received: 24 August 2020 / Accepted: 3 March 2021 / Published online: 10 March 2021

Abstract

The Upper Ordovician Zhe-Gan Platform was a short-lived carbonate platform that formed near the northern margin of the Cathaysian Land of the South China Block. The Zhe-Gan Platform is less well understood than the adjacent Yangtze Platform due to the absence of detailed sedimentological study as well as the structural complexity of the area. The aim of this study was to reconstruct the Zhe-Gan Platform based on detailed facies analysis of the middle to upper Xiazhen Formation. A total of 24 shallowing-upward depositional cycles (C1–24) are identified and subdivided into three types based on the vertical association of facies: (1) mixed carbonate–clastic subtidal cycles; (2) carbonate subtidal cycles; and (3) peritidal-capped subtidal cycles. The reconstructed depositional model indicates a ramp-type, mixed siliciclastic–carbonate platform, generally similar to other Late Ordovician carbonate platforms characterised by dominant skeletal grains, less common ooids, and an absence of skeletal barrier reefs. The newly developed Late Ordovician ramp-type carbonate platforms could have been induced by the evolution of skeletal organisms and the accompanying palaeoceanographic changes prior to the Hirnantian glaciation. The complex palaeogeography of the South China Block would have influenced the co-occurrence of the Xiazhen carbonate platform and black shales of the adjacent Yangtze Platform on the same block during the Late Ordovician.

Keywords Zhe-Gan Platform · Mixed siliciclastic–carbonate ramp · Upper Ordovician · South China Block

✉ Suk-Joo Choh
sjchoh@korea.ac.kr

Jino Park
jinopark@kangwon.ac.kr

Jeong-Hyun Lee
jeonghyunlee@cnu.ac.kr

Kun Liang
kliang@nigpas.ac.cn

1 Department of Geology, Kangwon National University, Chuncheon, Republic of Korea

2 Institute of Construction and Environmental Research, Handong Global University, Pohang, Republic of Korea

3 Department of Geological Sciences, Chungnam National University, Daejeon, Republic of Korea

4 State Key Laboratory of Palaeobiology and Stratigraphy, Nanjing Institute of Geology and Palaeontology and Centre for Excellence in Life and Paleoenvironment, Chinese Academy of Sciences, Nanjing, China

5 Department of Earth and Environmental Sciences, Korea University, Seoul, Republic of Korea

Introduction

Carbonate platforms in the early Palaeozoic developed mostly in the tropical to sub-tropical shallow-marine realms (Kiessling et al. 2003). Cambrian platform carbonates were mainly composed of non-skeletal allochems such as ooids and peloids with abundant microbial buildups (e.g., Webby et al. 2004; Pruss et al. 2010; Pratt 2010; Chen et al. 2011, 2014; Pratt et al. 2012; Lee et al. 2015). By the Early to Middle Ordovician, the Great Ordovician Biodiversification Event (GOBE) resulted in a sharp increase in both diversity and abundance of carbonate-secreting biota (Kiessling et al. 2003; Webby et al. 2004; Pruss et al. 2010). This led to a major change in carbonate depositional systems; for example, the importance of skeletal grains and reefs in carbonate platforms increased, whereas non-skeletal grains and microbialites diminished (Li and Droser 1997, 1999; Liu 2009; Pruss et al. 2010; Liu et al. 2011; Wright and Cherns 2016; Lee and Riding 2018).

The South China Block is a crucial region for understanding the evolution of early Palaeozoic carbonate depositional systems during and after the GOBE (e.g., Webby 2002; Webby et al. 2004). The Upper Ordovician carbonate successions of the Zhe-Gan Platform are exposed in Jiangxi and Zhejiang provinces, southeast China (Fig. 1). These carbonate rocks are known for their well-preserved, prolific occurrences of fossils with heavily calcified skeletons such as stromatoporoids, corals, and calcareous algae, as well as other diverse sessile and mobile taxa that flourished just before the end-Ordovician mass extinction event caused by the Hirnantian glaciation (e.g., Chen et al. 1987; Zhang et al. 2007; Lee et al. 2012). Various palaeontological and palaeoecological studies on these rocks during the last decade have improved our understanding of the Late Ordovician world: corals (Sun et al. 2014a, 2016, 2019; Dai et al. 2015; Liang et al. 2016; Zhang 2016); stromatoporoids (Jeon et al. 2020b); bryozoans (Zhang et al. 2018); *Amsassia* (Sun et al. 2014b; Lee et al. 2016b, 2019b); trilobites (Lee 2013); sponges (Park et al. 2015); reef communities (Kwon et al. 2012; Li et al. 2015; Lee et al. 2016a, 2019a; Jeon et al. 2020a); and cryptic communities (Park et al. 2017b), though sedimentological studies are still lacking.

The main objective of this study is the reconstruction and re-evaluation of the Xiazhen Formation of the Zhe-Gan Platform, which has been overlooked in comparison

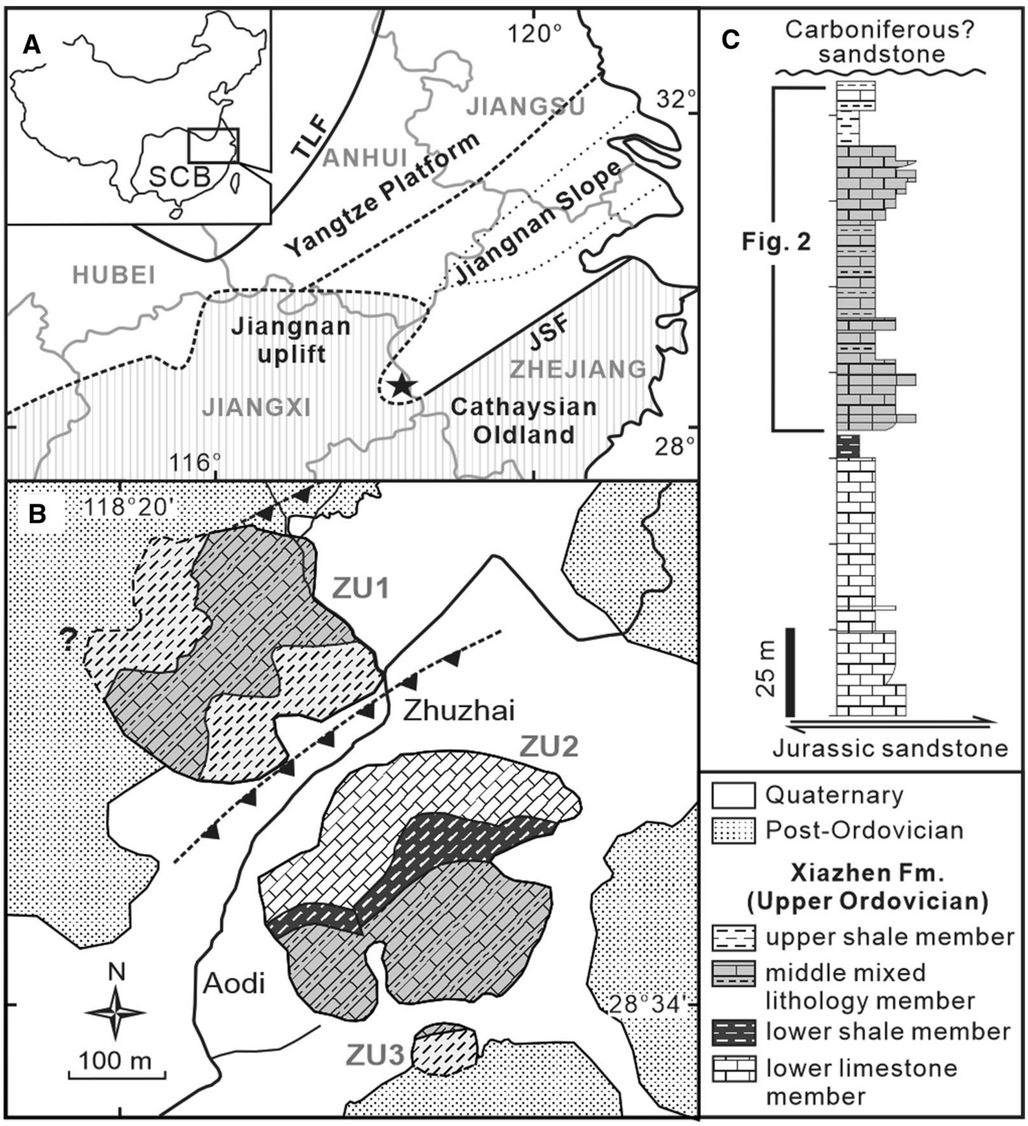

Fig. 1 **a** Palaeogeographic map of the South China Block during the Late Ordovician. The study area (the Zhuzhai section) is marked by a star (SCB = South China Block, TLF = Tan–Lu Fault, JSF = Jiangshan–Shaoxing Fault). Modified after Chen et al. (2018). **b** Geologic map of the study area around Zhuzhai village, Jiangxi Province. **c** Simplified lithological column of the Xiazhen Formation. The formation at Zhuzhai is in faulted contact with the underlying Jurassic sandstone of the Linshan Group and is disconformably overlain by the lower Carboniferous (?) Yejiatang Formation. Modified after Lee et al. (2012)

with the adjacent, well-known Yangtze Platform. This study examines the mixed carbonate and clastic succession of the middle to upper Xiazhen Formation at the Zhuzhai section in Yushan, Jiangxi Province, China and presents a general depositional model based on a detailed facies analysis (process-based approach). Improved knowledge of carbonate platform development on the South China Block prior to the Hirnantian glaciation event is useful to clarify the palaeogeography and palaeoceanography of the South China Block and to determine the key depositional features of Late Ordovician carbonate depositional systems.

Geologic setting and methods

The South China Block was located in a tropical realm of peri-Gondwana during the Late Ordovician (Kiessling et al. 2003; Torsvik and Cocks 2017; Scotese and Wright 2018) and consisted of four major geographical regions; these are, from northwest to southeast, the Yangtze Platform, the Jiangnan Slope, the Zhujiang Basin, and the Cathaysian Land (Rong and Chen 1987; Zhan et al. 2002; Li et al. 2004; Zhang et al. 2007; Chen et al. 2018). The Zhe-Gan Platform is suggested to have developed in an intracontinental basin of the Zhujiang Basin during the Late Ordovician (Fig. 1a; Zhan et al. 2002; Li et al. 2004; Zhang et al. 2007). Most of the Upper Ordovician carbonate (the Xiazhen and Sanjushan formations) and clastic (the Changwu Formation) successions of the Zhe-Gan Platform are located between the NE-striking Qiuchuan–Xiaoshan and Jiangshan–Shaoxing faults (Zhang et al. 2007, Fig. 2–1), and these successions are not well correlated due to the rarity of age-indicative fossils. This lack of correlation hampers detailed sedimentological studies of these lithologic units, as well as an understanding of the Zhe-Gan Platform (Lee et al. 2012).

The Xiazhen Formation, the focus of this study, is best exposed at Zhuzhai, 15 km southeast of Yushan and 7 km southwest from its type section located near Mt. Tashan (Zhan et al. 2002; Zhang et al. 2007). At Zhuzhai, the formation crops out with a gentle dip of 15–25° around three small hills, designated the ZU1, ZU2, and ZU3 subsections from NW–SE, where the formation overlies Jurassic clastic deposits and occurs as a thrust outlier or klippe (Fig. 1b). The Xiazhen Formation is divided into four informal members, which are, in ascending order, the lower limestone member (~ 75 m thick), the lower shale member (~ 8 m thick), the middle mixed lithology member (~ 85 m thick), and the upper shale member (~ 30 m thick) (Fig. 1c; Lee et al. 2012). The middle mixed lithology member is further subdivided into the lower limestone (~ 25 m thick), middle marlstone (~ 30 m thick), and upper limestone (~ 26 m thick) submembers based on their dominant lithology (Fig. 2). The entire Xiazhen Formation is disconformably overlain by Carboniferous (?) deposits at ZU3 (Zhang et al. 2007). The age of the Xiazhen Formation is only poorly defined (Zhang et al. 2007): the graptolite *Anticostia uniformis*, indicating a late Katian age, was recently found in the lower part of the upper shale member at ZU1 (Chen et al. 2016); and a specimen of a clathrodictyid stromatoporoid, which first appeared in the early Katian (Nestor and Webby 2013), was collected from the middle part of the lower limestone member at ZU2 (Jeon et al. 2020b). Based on these limited data, the Xiazhen Formation is interpreted to have accumulated throughout the Katian.

This study mainly considers the middle mixed lithology and upper shale members of the Xiazhen Formation (Fig. 2). The studied interval was measured in detail and about 300 samples were collected at vertical spacings of less than 20 cm in carbonate intervals to 5 m in clastic parts of the succession. Sedimentary structures and types of large (> 1 cm) fossils were described in the field. Sedimentary textures and allochems were described from 250 large-format (54 × 76 mm) and 50 standard-format (28 × 48 mm) thin sections cut perpendicular to bedding. The relative proportions of constituents were visually estimated from outcrop photographs and thin sections (Fig. 2; Matthew et al. 1991; Flügel 2004, p. 254–262). The 'white card technique' (Folk 1987) was routinely used for recognizing poorly preserved textures of stromatoporoids and calcimicrobes.

Middle mixed lithology and upper shale members of the Xiazhen Formation

The middle to upper Xiazhen Formation is divided into eight depositional facies on the basis of lithology, sedimentary structures and textures, grain constituents, and vertical variations (Table 1). There are seven facies associations: (1) massive clastic mudstone (Fig. 3a); (2) limestone–clastic mudstone couplets (Fig. 3b, c); (3) lime mudstone to wackestone (Fig. 3d); (4) skeletal and peloidal wackestone to packstone (Fig. 3e); (5) peloidal, skeletal, and intraclastic packstone to grainstone (Fig. 3f); (6) laminated marlstone (Fig. 3g, h); (7) microbial laminite (Fig. 3i); and a non-cyclic facies of (8) stromatoporoid–coral biostromes (Fig. 4).

The middle mixed lithology and upper shale members are characterised by skeletal limestone and frequent clastic interbeds (Fig. 2; Table 1). The lower and upper limestone submembers of the middle mixed lithology member mostly consist of subtidal carbonate facies with limestone–clastic mudstone couplets; lime mudstone to wackestone; skeletal and peloidal wackestone to packstone; and peloidal, skeletal, and intraclastic packstone to grainstone, with minor massive clastic mudstone and peritidal microbial laminite. Diverse skeletal allochems are observed in the carbonate facies, including dasyclad green algae, diverse clathrodictyid and

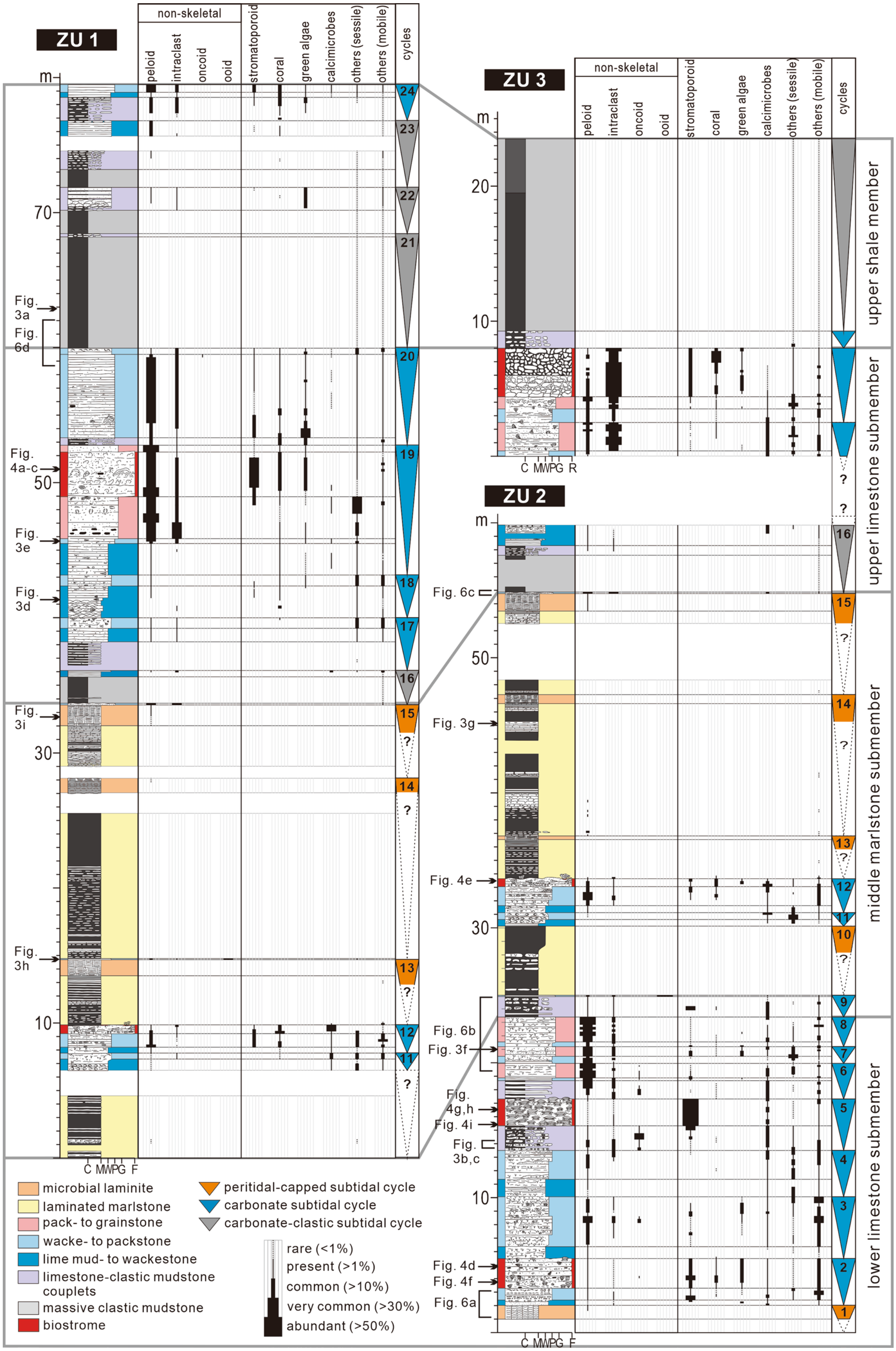
ZU 1
ZU 2
ZU 3
non-skeletal
peloid
intraclast
oncoid
ooid
stromatoporoid
coral
green algae
calcimicrobes
others (sessile)
others (mobile)
cycles
upper shale member
upper limestone submember
middle marlstone submember
lower limestone submember
microbial laminite
laminated marlstone
pack- to grainstone
wacke- to packstone
lime mud- to wackestone
limestone-clastic mudstone couplets
massive clastic mudstone
biostrome
peritidal-capped subtidal cycle
carbonate subtidal cycle
carbonate-clastic subtidal cycle
rare (<1%)
present (>1%)
common (>10%)
very common (>30%)
abundant (>50%)

◂**Fig. 2** Lithological logs and vertical distribution of allochem components and fossils, depositional facies, and shallowing-upward cycles in the middle to upper Xiazhen Formation in the Zhuzhai section. (C = claystone; M = lime mudstone; W = wackestone; P = packstone; G = grainstone; F = floatstone; R = rudstone)

labechiid stromatoporoids, diverse tabulate and rugose corals, molluscs, calcimicrobes, tetradiids, brachiopods, *Amsassia*, trepostome and cryptostome bryozoans, crinoid ossicles, *Solenopora*, trilobites, ostracods, *Bajgolia*, monaxial spicules, and non-lithistid demosponge networks (Table 1; see Lee et al. 2012; Sun et al. 2014a, b, 2016, 2019; Dai et al. 2015; Liang et al. 2016; Zhang 2016; Zhang et al. 2018; Jeon et al. 2020b). Common non-skeletal allochems in the same intervals include peloids, intraclasts consisting of diverse facies, and oncoids with diverse fossil nuclei. In contrast, the middle marlstone submember and upper shale member are composed of mixed carbonate–siliciclastic subtidal to peritidal deposits of clastic mudstone (massive clastic mudstone and laminated marlstone) and limestone (limestone–clastic mudstone couplets, lime mudstone to wackestone, skeletal and peloidal wackestone to packstone, and microbial laminite) facies. Here, occurrences of skeletal fossils and burrows are substantially reduced or nearly absent, although diverse mouldic fossils including whole to disarticulated brachiopods, trilobites, bivalves, nautiloids, and crinoids occur in the upper shale member (e.g., Zhan et al. 2002; Lee et al. 2012; Lee 2013). Carbonate interbeds contain diverse fossils similar to those of the limestone-dominated submembers (Fig. 2).

Depositional cycles

A total of 24 shallowing-upward depositional cycles (C1–24) are identified in the middle to upper Xiazhen Formation (Fig. 2). These cycles are subdivided into three types, based on the vertical association of facies: (1) mixed carbonate–clastic subtidal cycles; (2) carbonate subtidal cycles; and (3) peritidal-capped subtidal cycles (Fig. 5). Mixed carbonate–clastic subtidal cycles comprise both carbonate- and clastic-dominated subtidal facies including the massive clastic mudstone, limestone–clastic mudstone couplets, lime mudstone to wackestone, and skeletal and peloidal wackestone to packstone facies, and always begin with the massive clastic mudstone facies. Carbonate subtidal cycles are characterised by rhythmical associations of subtidal carbonate facies devoid of clastic mudstone facies, including limestone–clastic mudstone couplet; lime mudstone to wackestone; skeletal and peloidal wackestone to packstone; and peloidal, skeletal, and intraclastic packstone to grainstone facies in ascending order. Peritidal-capped subtidal cycles consist of the microbial laminite and laminated marlstone facies and typically show evidence of subaerial exposure (e.g., prism and desiccation cracks) at the tops of cycles with occasional quartzose sandstones and oolitic grainstones (Lee et al. 2012, Fig. 15). The mixed carbonate–clastic subtidal, carbonate subtidal, and peritidal-capped subtidal cycles reflect stacking of depositional facies in deeper, moderate, and shallower environmental settings, respectively (e.g., Bova and Read 1987; Osleger 1991; Pope 2014).

Lower limestone submember of the middle mixed lithology member

This submember mostly consists of subtidal carbonate cycles (C2–8), except for the lowermost peritidal-capped cycle (C1). An abrupt facies shift from the microbial laminite facies to the lime mudstone to wackestone facies, together with a distinct erosion surface, is well defined between the peritidal-capped (C1) and the subsequent carbonate subtidal cycle (C2) (Fig. 6a). The carbonate subtidal cycles (C2–8) consist of a cyclic association of carbonate subtidal facies, showing an upward reduction in cycle thickness from 3.5–5.5 to 1.2–4 m (Figs. 2 and 6b). A minor influx of muddy clastic sediments occurs in some of the upper subtidal cycles (C5 and C6).

The lowermost peritidal-capped cycle, though only identified as a single shallow microbial laminite facies above covering soil (Figs. 2 and 6a), possibly indicates that carbonate sedimentation was reactivated and the platform became substantially shallower, considering that the deeper clastic mudstone (massive clastic mudstone facies) mainly constitutes the underlying lower shale member (Fig. 1c; Lee et al. 2012). The facies arrangement and stacking pattern of the carbonate subtidal cycles (C2–8) suggest that the lower cycles (C2–4) formed in a low- to moderate-energy subtidal environment, whereas the upper cycles (C5–8) were deposited in a wider range of low- to high-energy subtidal settings in a shallower environment. Hence, the lower limestone submember is interpreted as shallow-marine subtidal deposits, showing an overall shallowing-upward trend with the renewed clastic influx, and eventually grading into the overlying middle marlstone submember (Fig. 6b).

Middle marlstone submember of the middle mixed lithology member

The depositional cycles in this submember (35 m thick) are composed of combined peritidal-capped subtidal and carbonate subtidal cycles (C9–15). In contrast to the rhythmic cyclical packages in the subtidal successions below, the lower part (C9–12) of this submember shows a different stacking pattern. The lowermost C9 is entirely composed of the limestone–clastic mudstone couplets facies, with alternating thin-bedded silty mudstone and bioclastic wackestone to grainstone interbeds similar to those of C8 (Fig. 6b). The

Table 1 Summary of depositional facies in the middle to upper Xiazhen Formation

Facies	Description		Interpretation
	Sedimentary structure and textures	Allochem composition	
Cyclic facies			
Microbial laminite	Light grey to dark dray Wavy or crinkled lamination consisting of thicker lighter peloidal micritic thin bed to lamina and thinner darker silty micritic or dolomitic lamina Common fenestrae or large (~3 cm) vuggy pores filled with calcite cements Common desiccation and prism cracks Local cm-scale microbialites consisting of banded or botryoidal micritic clumps	Common peloids	**Upper intertidal to supratidal microbial mats** (Demicco and Hardie 1994; Grimwood et al. 1999; Riding 2000; McLaughlin et al. 2004; Holland and Patzkowsky 2009, 2012; Pratt 2010; Husinec 2016)
Laminated marlstone	Grey to dark grey Lenticular, parallel, and low-angle X-lamination consisting of graded lighter calcareous silty/sandy mudstone lamina and overlying darker homogeneous mudstone lamina Common intercalations of either erosional based, single to multiple graded silty sandstone or silty oolitic packstone laminae to thin beds, or massive to sparsely laminated lime mudstone thin beds or nodules Local disturbed strata with dewatering structure Local polygonal desiccation cracks at the top of facies intervals Local tunneled horizontal to vertical burrows filled with lighter silty micritic sediment or cement	Rare peloids and whole to disarticulated fossils including ostracods, trilobites, brachiopods, sponge spicule networks Common radial ooids (< 1 mm in diameter) in thin graded interbeds Common quartz silts to medium-grained rounded sands in certain interbeds	**Peritidal to subtidal environments** Represents a combination of several different facies, but classified as one facies due to limited outcrop observation and fragile nature of mudrocks Depositional processes include: (1) Settling of muddy sediments (Potter et al. 2005); (2) Waning currents, such as tides, waves, or a combination of both (e.g., Potter et al. 2005; Schieber 2016); (3) Wave-enhanced sediment-gravity flows (Macquaker et al. 2010); (4) Storms (graded thin beds) (e.g., Aigner 1985); (5) Tidal currents (lenticular beddings)
Peloidal, skeletal, and intraclastic pack- to grainstone	Grey to dark grey Thin to medium bedded Stylolite-enhanced irregular erosional or stylolitic contacts Common well-rounded or micrite-enveloped allochems Some mottled or sub-horizontal to vertical burrows Some microbial encrustation of intraclasts or fossil fragments	Common to abundant peloids, rounded intraclasts, fragmented fossils including dasyclads, calcimicrobes, molluscs, stromatoporoids, tetradiids, *Amsassia*, crinoid ossicles, bryozoans Rare to some *Solenopora*, tabulate and rugose corals, brachiopods, monaxial and triaxial spicules, trilobites, ostracods, oncoids	**Deposition of high-energy peloidal** and **skeletal shoals or flats** (Semeniuk 1973; Grimwood et al. 1999; McLaughlin et al. 2004) Abundant dasyclads indicate deposition in euphotic, shallow-water conditions (Johnson and Sheehan 1985; Flügel 2004; Kröger et al. 2020)

Table 1 (continued)

Facies	Description		Interpretation
	Sedimentary structure and textures	Allochem composition	
Skeletal and peloidal wacke- to packstone	Grey to dark grey Thin to thick bedded Contacts enhanced by stylolite or dissolution seam Common mottled burrows Local pelletoidal textures with monaxial spicules Common microbial encrustation of intraclasts or fossils	Common peloids, whole to fragmented fossils including molluscs, calcimicrobes, stromatoporoids, corals, dasyclads, *Amsassia*, tetradiids, bryozoans, brachiopods Rare to some crinoid ossicles, *Solenopora*, monaxial spicules, ostracods, trilobites, small rounded micritic intraclasts, oncoids	**Deposition in moderate-energy open subtidal environments** (Semeniuk 1973; Grimwood et al. 1999; Holland and Patzkowsky 2009, 2012; Husinec 2016) Deposition within the upper euphotic zone (Flügel 2004)
Lime mud- to wackestone	Dark grey Thin to thick bedded or nodular bedded Contacts enhanced by stylolite or dissolution seam Local mottled bioturbation overlapped by tubed burrows	Rare to some peloid and small micritic intraclasts, whole to disarticulated fossils including molluscs, *Amsassia*, tetradiids, calcimicrobes, stromatoporoids, corals, crinoids, brachiopods, *Solenopora*, dasyclads, sponge spicules or spicule networks, ostracods, trilobites	**Deposition in low-energy subtidal environments** (Semeniuk 1973; Park et al. 2015; Husinec 2016) Deposition within the photic zone (Flügel 2004)
Limestone-clastic mudstone couplet	<u>Wacke- to packstone-clastic mudstone couplet subfacies</u> Alternation of grey to dark grey massive wacke- to packstone and dark grey clastic mudstone thin (1–15 cm) beds Continuous or nodular layered Common mottled burrows Occasional intercalation of graded packstone laminae with erosional surface Common to rare graded silty laminae in mudstone interbeds Decrease upward of clastic mudstone thickness	Locally common concentric to lobate, porostromate-type oncoids with diverse nuclei, whole to fragmented fossils of molluscs, calcimicrobes, dasyclads, stromatoporoids, corals, *Solenopora* Rare brachiopods, *Amsassia*, ostracods, trilobites, bryozoans, tetradiids, crinoid ossicles	**Alternating deposition of muddy carbonate** and **settling** and **reworking of suspended muds across low (LM-M) to moderate-energy (W/P-M) subtidal environments** (e.g., McLaughlin et al. 2004; Carlucci et al. 2014)
	<u>Lime mudstone-clastic mudstone couplet subfacies</u> Alternation of dark grey massive lime mudstone and dark brownish grey massive clastic mudstone thin (1–15 cm) beds Continuous or nodular layered Decrease upward of clastic mudstone thickness	Rare sponge spicule networks, gastropods, trilobites, a branching tabulate coral *Kolymopora*	

Table 1 (continued)

Facies	Description		Interpretation
	Sedimentary structure and textures	Allochem composition	
Massive clastic mudstone	Deep greenish grey to brownish grey or reddish brown Massive non-fissile homogeneous claystone Local faint parallel lamination consisting of lighter and darker claystone laminae Local *in-situ* fossil-enriched horizons	Rare scattered silt quartz increased upward Moldic whole to disarticulated remains of brachiopods, trilobites, bivalves, nautiloids, crinoid stem and holdfasts	**Settling of suspended detrital muds** (Potter et al. 2005) Favourable conditions for the preservation of benthic organisms due to rapid deposition of sediments (e.g. O'Brien et al. 1994)
Non-cyclic facies			
Stromatoporoid-coral biostrome	<u>Domal stromatoporoid-coral biostrome subfacies</u> Grey to dark grey low-relief biostromal reef complex composed of stromatoporoid-coral framestone and coral rudstone Peloidal and bioclastic pack- to grainstone matrix	Major reef components: laminar-encrusting (low to high domical) *Clathrodictyon* and colonial coral *Plasmoporella*, Minor reef components: *Ecclimadictyon*, *Agetolites*, *Heliolites*, *Catenipora*, solitary rugosans, and dasyclad *Vermiporella* Allochem in matrix: common to abundant peloids and intraclasts; common dasyclads and molluscs; rare to some crinoid ossicles, bryozoans, monaxial spicules, ostracods, trilobites, tetradiids	**Biostrome formed on high-energy subtidal deposits** Abundant dasyclads indicate deposition in euphotic, shallow-water conditions (Johnson and Sheehan 1985; Flügel 2004; Kröger et al. 2020)
	<u>Columnar branching stromatoporoid-coral biostrome subfacies</u> Dark grey biostromal reef complex composed of stromatoporoid-coral bioherm and floatstone Local small (cm-scale) microbial bioherm consisting of *Ortonella* Bioclastic wacke- to packstone matrix	Major reef components: cylindrical branching *Clathrodictyon* Minor reef components: *Ecclimadictyon*, *Agetolites*, *Catenipora*, *Heliolites*, solitary rugosans, calcimicrobes Allochem in matrix: rare to common dasyclads, molluscs, tetradiids, calcimicrobes *Subtifloria* and *Hedstroemia*; rare to some crinoid ossicles, brachiopods, bryozoans, *Solenopora*, ostracods, trilobites; rare to some peloids and intraclasts	**Biostrome formed on moderate-energy subtidal deposits** Rare to common dasyclads indicate deposition within the photic zone (Johnson and Sheehan 1985; Flügel 2004; Kröger et al. 2020)
	<u>Domal stromatoporoid biostrome subfacies</u> Light grey to grey biostromal framestone composed of exclusively large low domical (<1 m) labechiid stromatoporoids Lime mud- to wackestone matrix	Major reef contributors: laminar-encrusting (domical) *Stylostroma* Allochems in matrix: rare to common calcimicrobes *Ortonella* and *Subtifloria*, molluscs; rare tetradiids, ostracods, trilobites, bryozoans, *Tryplasma*; rare peloids and intraclasts	**Biostrome formed on low-energy subtidal deposits** Absence of dasyclads probably indicates deposition below the photic zone (Johnson and Sheehan 1985; Flügel 2004; Kröger et al. 2020)

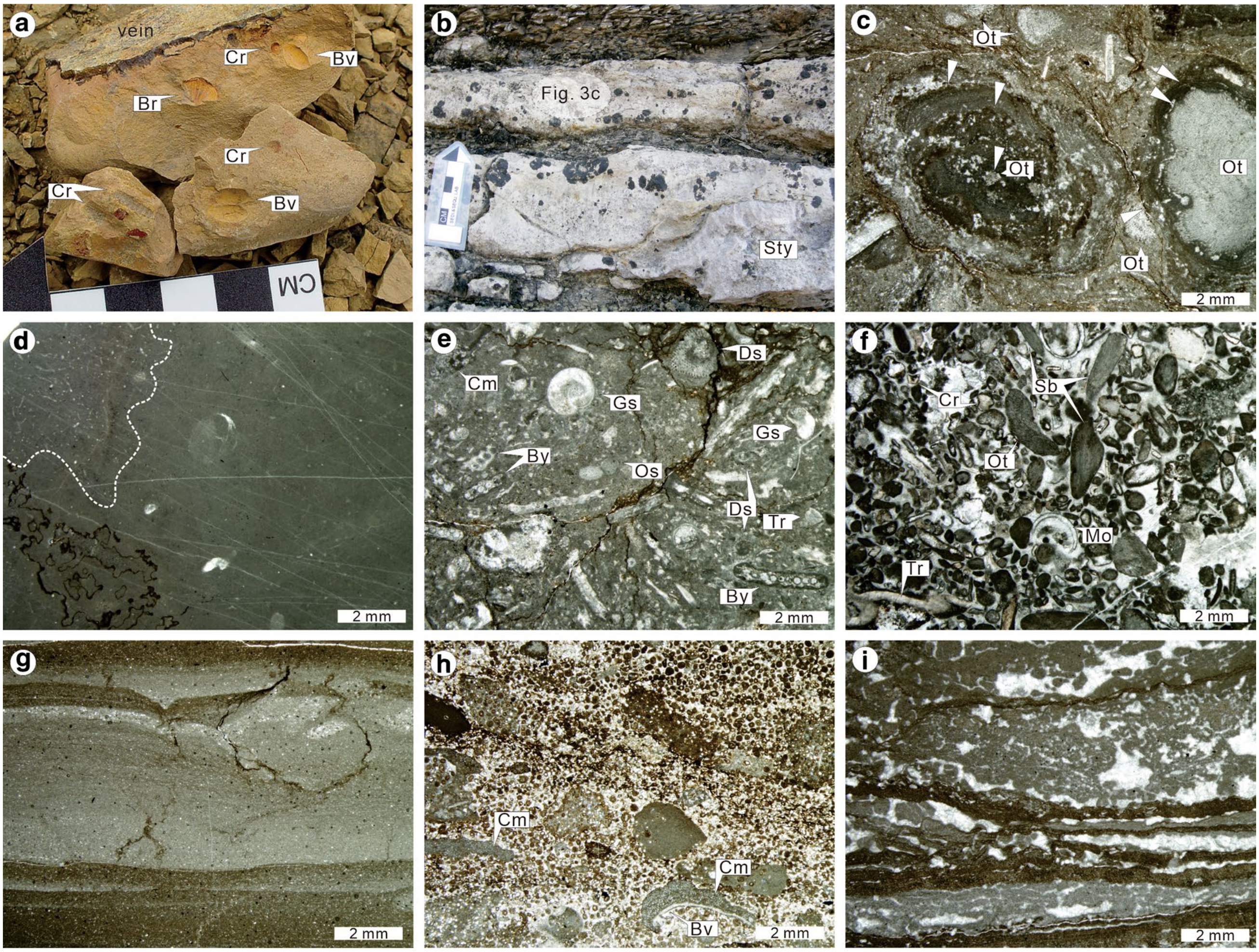

Fig. 3 Cyclic depositional facies of the middle to upper Xiazhen Formation. **a** Photograph of massive clastic mudstone in the upper shale member at ZU1 with moulds of brachiopods (Br), bivalves (Bv), and crinoids (Cr). **b** Photograph of limestone–clastic mudstone alternations, containing a *Stylostroma* stromatoporoid (Sty) in the lower wackestone to packstone layer (scale in centimetres). **c** Photomicrograph of concentric to lobate oncoids with multiple encrustations (white arrows) (Ot = *Ortonella*). **d** Photomicrograph of the lime mud- to wackestone facies containing a poorly preserved spicular network (dotted line in the upper left corner), and burrows filled with micritic sediment and cement. **e** Photomicrograph of the skeletal and peloidal wacke- to packstone facies including whole to fragmented remains of cryptostome bryozoans (By), gastropods (Gs), dasyclads (Ds), trilobites (Tr), and ostracods (Os). **f** Photomicrograph of the peloidal, skeletal, and intraclastic pack- to grainstone facies composed of rounded diverse calcimicrobes including *Subtifloria* (Sb) and *Ortonella* (Ot), crinoid ossicles (Cr), mollusc fragments (Mo), trilobites (Tr), peloids, and diverse intraclasts. **g** Photomicrograph of laminated marlstone facies showing lamina sets of normally graded light grey silty calcareous laminae with erosional bases and overlying dark grey homogeneous mudstone laminae. **h** Photomicrograph of silty oolitic pack- to grainstone thin bed intercalated within the laminated marlstone facies and composed of small radial ooids with common quartz nuclei, intraclasts, and calcimicrobes (Cm) encrusting a bivalve (Bv). **i** Photomicrograph of microbial laminite facies containing fenestral pores

overlying C10 begins with an oolitic grainstone bed, overlain by thick beds of the laminated marlstone facies that coarsen upward to medium-grained sandstone, and are then overlain by the lime mudstone facies of C11 with a sharp contact. Thinner (1–2 m thick) carbonate subtidal cycles (C11 and C12), similar to those of the lower submember, were temporarily developed between thicker (4–12.5 m thick) peritidal-capped subtidal cycles (C10 and C13–15) (Fig. 2). The three peritidal-capped subtidal cycles in the mid–upper parts (C13–15) are mostly composed of the laminated marlstone facies and are capped by cracked microbial laminite facies (Fig. 6c). These clastic mudstone-dominated peritidal cycles are only tentatively defined, as mudstones may preserve complex sedimentary processes (Table 1; e.g., Macquaker et al. 2010; Schieber 2016), although the microbial laminites at the top of each cycle suggest upper intertidal to supratidal environments and help to define the depositional cycle cap (Fig. 2; e.g., Bova and Read 1987; Demicco and Hardie 1994; Pratt 2010). The composition of the microbial laminites facies successively changes upward: clastic

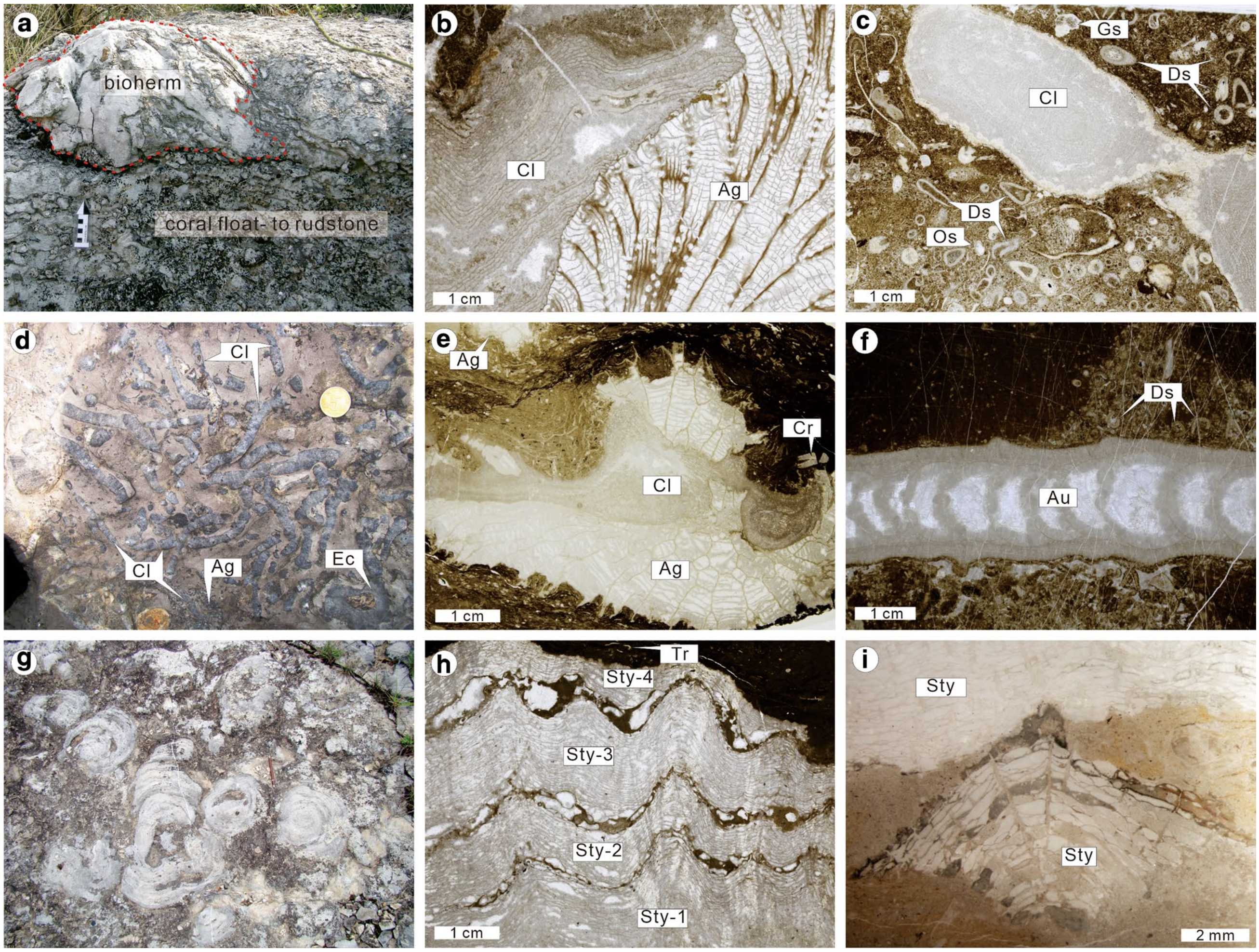

Fig. 4 Stromatoporoid–coral biostrome facies. **a** Photograph of the domical stromatoporoid–coral biostrome subfacies. Note a small bioherm (red dotted line) consisting of laminar-encrusting domical *Clathrodictyon* stromatoporoids and some corals surrounded by coral floatstone to rudstone (scale in centimetres). **b** Photomicrograph of a bioherm, consisting of *Clathrodictyon* (Cl) and *Agetolites* (Ag), in the domical stromatoporoid–coral biostrome subfacies. **c** Photomicrograph of packstone to grainstone matrix in the domical stromatoporoid–coral biostrome, containing a cylindrical *Clathrodictyon* stromatoporoid (Cl), dasyclads (Ds), gastropods (Gs), ostracods (Os), and small peloids. **d** Photograph of the columnar branching stromatoporoid–coral biostrome subfacies with *Clathrodictyon* (Cl), *Ecclimadictyon* (Ec), and *Agetolites* (Ag) in the bedding plane (the coin for scale is 20.5 mm in diameter). **e** Photomicrograph of the branching stromatoporoid–coral biostrome subfacies, showing *Clathrodictyon* (Cl) encrusted by an *Agetolites* (Ag), surrounded by bioclastic wackestone with a crinoid fragment (Cr). **f** Photomicrograph of wackestone to packstone matrix in the branching stromatoporoid–coral biostrome, containing a columnar aulaceratid (Labechiida) stromatoporoid (Au), dasyclads (Ds), and other fossil fragments. **g** Bedding-plane photograph of the domical stromatoporoid biostrome subfacies (the mechanical pencil for scale is 14.2 cm long). **h** Photomicrograph of encrusted laminar *Stylostroma* stromatoporoids (Sty-1–4), surrounded by micritic sediments with trilobite (Tr) fragments. **i** Photomicrograph of *Stylostroma* stromatoporoids (Sty) surrounded by lime mudstone to wackestone matrix sediments in the domical stromatoporoid biostrome, taken using the white card method

mud-dominated in C13; mixed clastic–carbonate in C14; and carbonate-dominated in C15 (Lee et al. 2012, Fig. 15).

This submember is interpreted as having been deposited in subtidal to peritidal environments with a mixed influx of both clastic and carbonate sediments. The development of the laminated marlstone facies indicates a clastic influx, resulting in suppression of carbonate deposition in the shallow-marine environment and a break of the rhythmical stacking pattern of previous carbonate subtidal cycles (C2–8) (Fig. 2). The upward increase in carbonate in the microbial laminites facies of peritidal-capped cycles (C13–15), as well as the transition into the upper limestone submember, suggest diminished clastic supply.

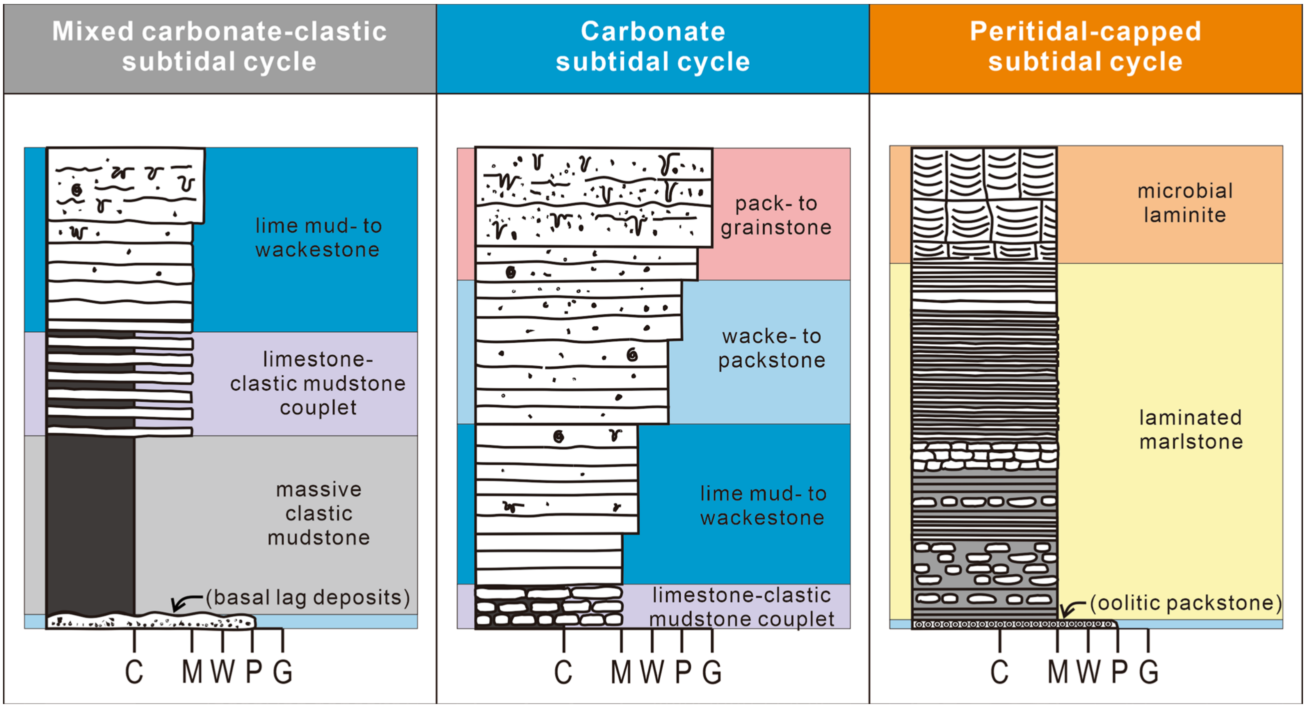

Fig. 5 Three types of idealised metre-scale depositional cycles in the middle to upper Xiazhen Formation

Upper limestone submember of the middle mixed lithology member

The uppermost peritidal microbial laminites in the top of the middle marlstone submember are sharply overlain by thin (5–15 cm thick), uneven beds of intraclastic and bioclastic packstone, followed by the deeper subtidal massive clastic mudstone facies of the mixed carbonate–clastic subtidal cycle (C16) (Fig. 6c). This submember is 25 m thick and is composed of the lowermost mixed carbonate–clastic subtidal cycle (C16) and carbonate subtidal cycles (C17–20). These metre-scale cycles show an upward decrease in the proportion and/or disappearance of the deeper facies, the appearance of and/or increase in proportion of the shallower carbonate facies, and an overall increase in cycle thickness from 2.5–5 to 7.5–10 m (Fig. 2). A minor influx of muddy clastic sediments is recognised in the lower part (limestone–clastic mudstone couplets facies) of the uppermost subtidal cycle (C20), which is in turn overlain by the thicker massive clastic mudstone facies (C21) of the upper shale member (Fig. 6d).

The abrupt shift from the shallowest (microbial laminites facies in C15) to the deepest (massive clastic mudstone facies in C16) facies with basal lag deposits (i.e., thin packstone) suggests a rapid deepening event (Holland 1993), which resulted in a distinct change in the stacking patterns of facies and cycles (Fig. 2). Similar to the lower limestone submember, the stacking pattern of cycles in this submember shows a shallowing-upward trend of shallow-marine subtidal carbonate deposits. However, the overall increase in cycle thickness (C16–20), together with the deposition of thick, deeper massive clastic mudstone facies (C21) of the upper shale member above, is indicative of a gradational increase in accommodation space, thus suggesting a longer-term sea-level rise (e.g., Bova and Read 1987; Osleger 1991; Holland 1993; Batten Hender and Dix 2008; Pope 2014).

Upper shale member

This member is largely composed of mixed carbonate–clastic subtidal cycles (C21–23) and a thin carbonate subtidal cycle (C24). Clastic mudstone (massive clastic mudstone and limestone–clastic mudstone couplet facies) is the most dominant rock type in this member (Figs. 3a, b and 6d). The observed cycles in the member show an overall decrease in cycle thickness from 5–8.5 to < 4 m, in contrast to those of the underlying upper limestone submember (Fig. 2).

The development of a thick mixed carbonate–clastic subtidal cycle (C21) in the lower part of this member possibly indicates a further rise in relative sea-level and/or an increased influx of muddy clastic sediments after deposition of the underlying carbonate cycles. A facies shift from deeper to shallower facies and a decrease in cycle thickness in cycles C21–24 are interpreted to be a shallowing-upward stacking pattern from deeper clastic subtidal to shallower carbonate subtidal environments. A transition from deepening to shallowing cycles possibly occurred in C21, because

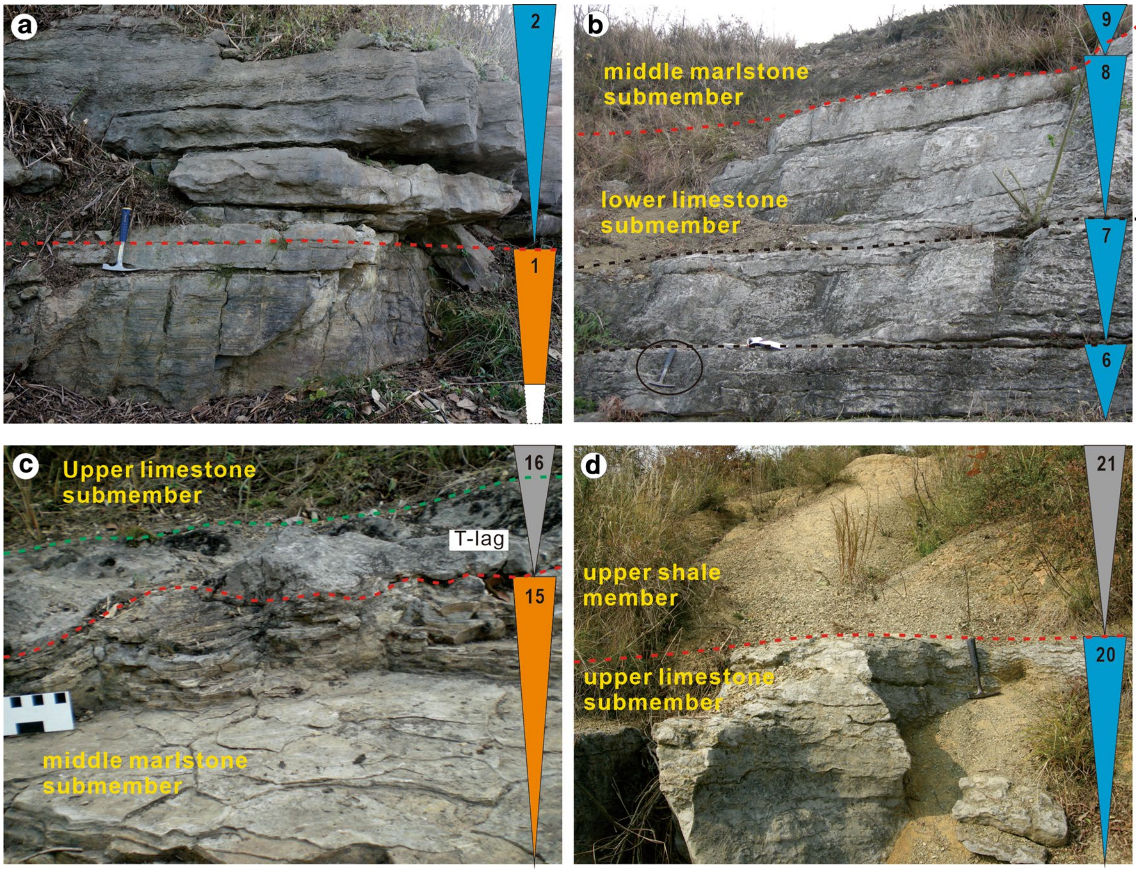

Fig. 6 Examples of depositional cycles and major cycle boundaries. **a** A distinct surface (red dotted line) between the underlying microbial laminite of a peritidal-capped subtidal cycle (C1) and the overlying lime mud- to wackestone and wacke- to packstone facies of a carbonate subtidal cycle (C2) in the basal part of the lower limestone submember (the hammer for scale is 28 cm long). **b** Boundary (red dotted line) between the underlying wacke- to packstone and pack- to grainstone facies of C6–8, bounded by flooding surfaces (black dotted lines), and the overlying wacke- to packstone–clastic mudstone of C9, forming the boundary between the lower limestone and middle marlstone submembers (the hammer for scale is 28 cm long). **c** Boundary (red dotted line) between the underlying microbial laminite of a peritidal-capped subtidal cycle (C15) and the overlying transgressive lag deposits (T-lag) and massive clastic mudstone facies of a mixed carbonate–clastic subtidal cycle (C16), forming the boundary between the middle marlstone and upper limestone submembers (scale in centimetres). **d** Boundary (red dotted line) between the underlying wacke- to packstone facies of C20 and the overlying massive clastic mudstone facies of C21, forming the boundary between the middle mixed lithology and upper shale members (the hammer for scale is 28 cm long)

this interval contains the thickest and deepest subtidal deposits in the middle to upper Xiazhen Formation (Fig. 2). Thus, this member is interpreted as deeper subtidal deposits formed during the drowning and resurgence of the carbonate platform.

Stromatoporoid–coral biostrome facies

Stromatoporoid–coral biostromes occur at four intervals in the middle mixed lithology member and are divided into three types on the basis of the dominant biota, associated fossils, and surrounding facies (Jeon et al. 2020b): (1) domical stromatoporoid–coral biostrome; (2) columnar branching stromatoporoid–coral biostrome; and (3) domical stromatoporoid biostrome subfacies (Table 1; Fig. 4). Generic names of corals follow Lee et al. (2012, Fig. 9) as well as Liang et al. (2016) for *Catenipora* and Sun et al. (2016) for *Agetolites*, and those of stromatoporoids are after Jeon et al. (2020a, b).

Domical stromatoporoid–coral biostrome subfacies

The domical stromatoporoid–coral biostrome subfacies consists of light grey to grey low-relief complexes with abundant small (< 1 m in diameter and high) bioherms and coral rubble (Fig. 4a). The main components of these bioherms are laminar-encrusting domical stromatoporoids (mainly *Clathrodictyon* with some *Ecclimadictyon*), various tabulate corals (including *Plasmoporella*, *Agetolites*, *Heliolites*, and *Catenipora*), solitary rugosans, and the dasycladalean

Vermiporella (Fig. 4b, c). These bioherms are laterally surrounded by bioclastic floatstone to rudstone with peloidal and bioclastic packstone to grainstone (Table 1; Fig. 4a, c). These subfacies only occurs in the upper part of the upper limestone submember at ZU1 intercalated within the peloidal, skeletal, and intraclastic packstone to grainstone facies. These subfacies laterally changes to a thinner bed of rudstone and floatstone with peloidal and skeletal packstone to grainstone at ZU3, interpreted as deposits flanking these bioherms (Fig. 2).

The diverse fossil fragments including common to abundant dasyclads, the dominance of encrusting sessile organisms, and the complex distribution of rudstone, as well as the packstone to grainstone matrix of these subfacies, collectively indicate that this unit formed in upper euphotic, high-energy, shallow-water conditions (e.g., Johnson and Sheehan 1985; Flügel 2004, p. 430–447; Pratt and Haidl 2008; Kröger et al. 2020). The absence of bioherms larger than 1 m in size and the presence of abundant coral rubble in these subfacies might be due to the general absence of effective binding organisms, except for some laminar-encrusting stromatoporoids (Jeon et al. 2020b). The distribution of these subfacies within the peloidal and skeletal packstone to grainstone facies suggests that the biostrome might have been located near a shoal environment.

Columnar branching stromatoporoid–coral biostrome subfacies

The columnar branching stromatoporoid–coral biostrome subfacies comprises dark grey organic-rich biostrome (framestone and floatstone) consisting mainly of in situ and reworked columnar *Clathrodictyon* with minor laminar-encrusting to domical *Ecclimadictyon*, and agetolitid, heliolitid, and halysitid tabulate corals (Table 1; Fig. 4d, e). Centimetre-scale bioherms exclusively composed of the calcimicrobe *Ortonella* (e.g., Pratt and Haidl 2008) are often developed near large sessile biota. The matrix is bioclastic wackestone to packstone with local mottled burrows (Table 1; Fig. 4f). Some peloids and angular to rounded lime mudstone to packstone intraclasts are also present. These subfacies occurs in two stratigraphic intervals in the lower limestone and middle marlstone submembers, both underlain by the wackestone to packstone facies (Fig. 2).

This biostrome subfacies is interpreted to have been formed in an upper euphotic, low- to moderate-energy subtidal environment, based on the diverse fossil assemblages and the surrounding wackestone to packstone matrix as well as the underlying wackestone to packstone facies (Jeon et al. 2020b). The dominance of the columnar *Clathrodictyon* in this biostrome subfacies, in contrast to the domical stromatoporoid–coral biostrome subfacies, might be attributed to an environmental change from a higher-energy grainy substrate to a lower-energy muddy substrate (Webby 2004; Park et al. 2017a).

Domical stromatoporoid biostrome subfacies

The domical stromatoporoid biostrome subfacies consist of dark grey to grey biostromes (framestone) exclusively composed of in situ large low domical labechiid *Stylostroma* (Fig. 4g–i). These biostromes are approximately 2 m thick, and their thickness and textures are laterally uniform over a distance of 200 m. The size of stromatoporoids commonly increases upward, from domical forms less than 20 cm in height and diameter to low domical forms 40 cm in height and 100 cm in diameter. The surrounding sediments are homogeneous lime mudstone to wackestone with some local mottled burrows, and contain various fossils (Fig. 4h, i; Table 1). These subfacies occurs in the middle part of the lower limestone submember and is gradationally underlain and sharply overlain by the wackestone to packstone–clastic mudstone alternations (Fig. 2).

The lime mudstone to wackestone matrix and the low diversity of the fossil assemblage in these subfacies indicate that this biostrome formed under low-energy subtidal environments below normal wave base. The absence of dasyclads in these subfacies may suggest a water depth below the upper euphotic zone (e.g., Johnson and Sheehan 1985; Flügel 2004, p. 430–447; Kröger et al. 2020).

Discussion

Depositional model of the Xiazhen Formation and its palaeogeographic implications

The middle to upper Xiazhen Formation preserves a mixed carbonate–clastic platform with a significant influx of muddy clastic sediments. The sedimentary facies of the Xiazhen Formation generally indicate inner-, middle-, and outer-platform environments (Fig. 7; Burchette and Wright 1992). The wide range of depositional environments, the absence of resedimented slope strata in the deepest shale facies, and the gradational facies shift forming subtidal to peritidal cyclic successions, collectively suggest a ramp-type platform environment. The biostromes in the Xiazhen Formation repeatedly developed throughout the succession in a wide range of environmental settings, from high-energy shallow to low-energy deeper subtidal environments without forming a thick barrier-reef complex (Fig. 7; Table 1). The occurrence of various sessile (i.e., stromatoporoids, corals, green algae, calcimicrobes, tetradiids, and *Amsassia*) and mobile shelly biota, as well as diverse biostromes, indicate that a variety of skeletal organisms rapidly appeared and inhabited shallow-marine environments, which substantially

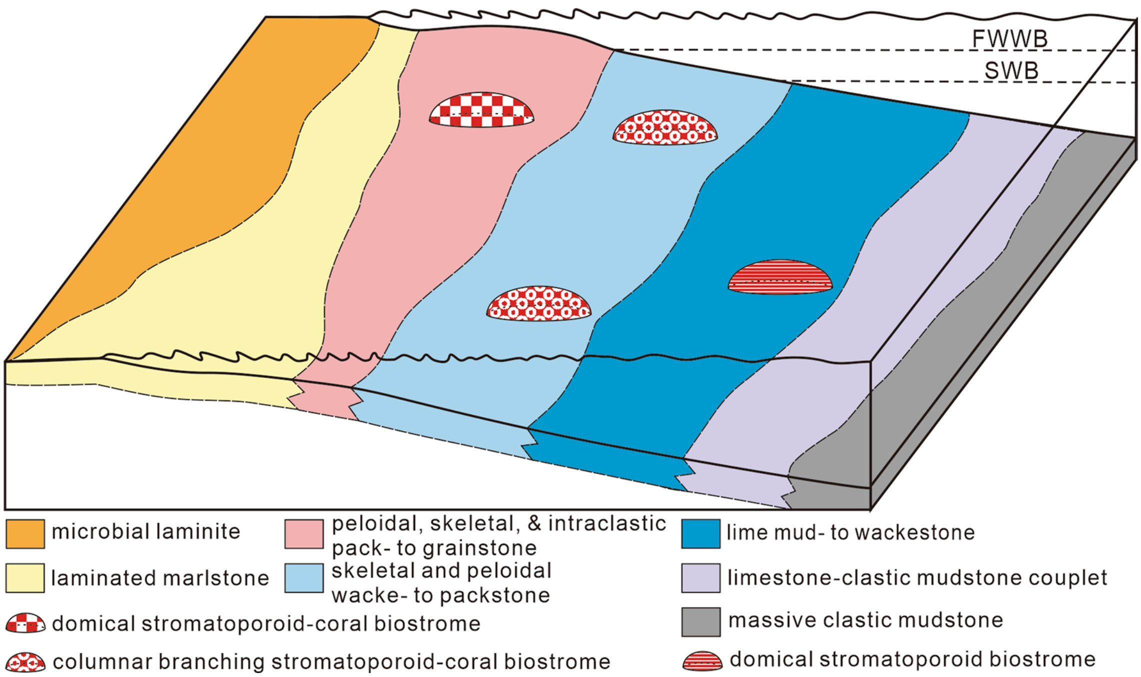

Fig. 7 Depositional model of the Xiazhen Formation, representing a mixed carbonate–clastic ramp-type platform ranging from peritidal to deep subtidal environments with a significant input of muddy clastic sediments (FWWB = fair weather wave base, SWB = storm wave base)

contributed to the development of carbonate facies. Carbonate deposition on the platform was punctuated by repeated clastic influxes, indicated by the recurrence of the clastic mudstone facies throughout the succession, possibly related to tectonic movement of the source area (e.g., Cathaysian Land; Li et al. 2004, 2015; Zhang et al. 2007; Chen et al. 2018).

Overall, the middle to upper Xiazhen Formation represents a decrease (cycles 1–15) and an increase (cycles 16–24) in accommodation space controlled by relative sea-level change (e.g., Bova and Read 1987; Osleger 1991; Holland 1993; Batten Hender and Dix 2008; Pope 2014). The abrupt facies shifts from carbonate to shale between the submembers, especially those between cycles C15–C16 and C20–C21, may suggest recurring drowning events (Schlager 1989, 1999) caused by rapid relative sea-level rise (e.g., Loi et al. 2010) or regional tectonic subsidence (Li et al. 2019), with possible time gaps between these cycles (Fig. 6c, d). For example, Li et al. (2020) suggested the existence of palaeokarst at the top of the middle mixed-lithology member (between cycles C20 and C21). Owing to the lack of biostratigraphic control, we cannot identify the significance of superposition by shale-dominated intervals. This should be investigated in future studies.

Deposition of the Upper Ordovician Zhe-Gan Platform is unique because most of the coeval successions in the adjacent Yangtze Platform are dominated by organic-rich black shale (the Wufeng Formation) deposited in deeper environments (e.g., Zhang et al. 2007; Chen et al. 2018). The lateral juxtaposition of platform and basin successions may indicate differential uplift of the southeastern part of the South China Block (i.e., the Cathaysian Land), which resulted in a break in the 'longstanding' platform–slope–basin pattern of the South China Block (Fig. 1a; Chen et al. 2018). The Zhe-Gan Platform has been suggested to have been a "rimmed" carbonate platform that developed on the active margin of the Cathaysian Land based on the proposed correlation of "inner-platform to lagoonal" deposits of the Xiazhen Formation, thicker "platform-margin" carbonates of the Sanjushan Formation, and outer-platform clastic sediments of the Changwu Formation (Li et al. 2004). However, the reconstructed Xiazhen depositional model presented here indicates a ramp-type platform. Our interpretation is corroborated by the published sedimentological logs of the Sanjushan Formation, which dominantly consists of argillaceous and bioclastic limestone devoid of massive reef facies (Zhan et al. 2002, Fig. 3) with slump sheets developed in slope environment (Li et al. 2019), thereby refuting the previous "rimmed platform" model (cf. Li et al. 2004).

The depositional model of the middle to upper Xiazhen Formation presented in this study could be a useful guide for further studies to reveal the stratigraphical relationship between the Xiazhen, Sanjushan, and Changwu formations of the Zhe-Gan Platform and to understand the palaeogeography of the South China Block. It has recently been suggested that cool-water depositional environments prevailed

Table 2 Summary of Upper Ordovician tropical to sub-tropical carbonate platforms. The white- and grey-coloured rows indicate carbonate and mixed siliciclastic–carbonate platforms, respectively

Age and formation	Palaeo-continent (Area)	Basin type	Platform type	Depositional environments					Sources
				Peritidal	Inner (lagoon or restricted)	Inner (shoal)	Middle (transition)	Outer	
Katian Xiazhen Fm	Gondwana (SE China)	Epicontinental active margin?	Ramp	Peloids Bioclasts	Ooids Bioclasts	**Peloids** **Bioclasts** **Intraclasts** Oncoids	**Bioclasts** Peloids Intraclasts Oncoids	Bioclasts Peloids Intraclasts	This study
Upper Katian Red River Fm	Laurentia (North Dakota, USA)	Epicratonic (Williston Basin)	Shelf (HST and LST)	**Intraclasts**	N/A	N/A	N/A	N/a	Husinec (2016)
			Shelf (TST)	Intraclasts	Bioclasts	**Bioclasts** **Peloids** Intraclasts	**Bioclasts** Peloids	Bioclasts Peloids	
Katian to Hirnantian carbonates of western Estonian	Baltica (Estonia)	Epicontinental passive margin	Ramp or shelf	N/A	N/A	**Bioclasts** Ooids Peloids	**Bioclasts**	Bioclasts Peloids	Harris et al. (2004)
Middle to upper Katian Montoya Group	Laurentia (New Mexico, Texas, USA)	Epicontinental passive margin	Ramp (TST ~ HST)	Intraclasts	Bioclasts	**Bioclasts** Peloids	**Bioclasts**	Bioclasts	Pope (2014)
Middle to upper Katian Bighorn Dolomite	Laurentia (Wyoming, USA)	Epicontinental passive margin	Ramp	Intraclasts	Bioclasts Intraclasts Peloids	Bioclasts	Bioclasts	**Bioclasts** Peloids	Holland and Patzkowsky (2009, 2012)
Cincinnatian (Katian) Series	Laurentia (Indiana, Ohio, Kentucky, USA)	Peripheral bulge of foreland basin	Ramp (HST)	Bioclasts		**Bioclasts**	**Bioclasts**	Bioclasts	Holland (1993)
			Ramp (TST)	N/a	Bioclasts	**Bioclasts**	**Bioclasts**	N/A	
Lower Katian Lianglitage Fm	Tarim (NW China)	Forebulge cratonic basin	Carbonate platform (HST)	Peloids	**Intraclasts** **Peloids** Bioclasts	**Intraclasts** **Bioclasts** **Ooids** Peloids	N/A	N/A	Gao and Fan (2014); Gao et al. (2014)
			Carbonate platform (TST)		Intraclasts Peloids Bioclasts	**Intraclasts** **Bioclasts** **Oncoids**	**Oncoids** Bioclasts	N/A	
Sandbian-Kantian Daylesford Limestone	Gondwana (NSW, Australia)	Forearc basin?	carbonate platform	N/a		**Bioclasts** **Intraclasts** Peloids Pisoids	**Bioclasts** Peloids	Bioclasts Peloids	Semeniuk (1973); Fergusson (2009)
Sandbian Bromide Fm	Laurentia (Oklahoma, USA)	Aulacogen (rift basin)	Distally steepened ramp (S3)	Bioclasts	Bioclasts Peloids	**Bioclasts**	**Bioclasts**	N/a	Carlucci et al. (2014)
			Distally steepened ramp (S1–2)		N/A	**Bioclasts**	**Bioclasts**	Bioclasts	

Table 2 (continued)

Age and formation	Palaeo-continent (Area)	Basin type	Platform type	Depositional environments					Sources
				Peritidal	Inner (lagoon or restricted)	Inner (shoal)	Middle (transition)	Outer	
Sandbian Lourdes Fm	Laurentia (Newfoundland, Canada)	Peripheral foreland basin	Ramp (HST)	Bioclasts Peloids Intraclasts	N/a	**Bioclasts**	**Bioclasts** **Intraclasts**	N/A	Batten Hender and Dix (2006, 2008)
			Ramp (TST)	N/A	N/A	**Oncoids** **Intraclasts** Bioclasts Superficial ooids Peloids	**Bioclasts** **Oncoids** Peloids Intraclasts Pisoids	N/A	
Sandbian Gull River and Coboconk fms	Laurentia (Ontario, Canada)	Epicratonic (St. Lawrence Platform)	Ramp	Intraclasts Peloids Ooids Oncoids Bioclasts	Peloids Bioclasts Ooids Intraclasts Oncoids	**Peloids** **Bioclasts** Intraclasts Oncoids	N/A	N/A	Grimwood et al. (1999)

on the Yangtze Platform of the South China Block during the Late Ordovician, based on the prevalence of the cool-water *Foliomena* brachiopod fauna, a positive shift of $\delta^{18}O$ values, and the absence of warm-water taxa and carbonate components such as ooids, green algae, sponges, stromatoporoids, and corals (Jin et al. 2018). However, as demonstrated here, the Zhe-Gan Platform contains sedimentary components distinct from those of the adjacent Yangtze Platform, suggesting that differences in the temperature and/or salinity of water masses may have influenced the region (e.g., Holmden et al. 1998). Our study suggests that the regional palaeogeography was more complex than previously interpreted.

Comparison of Late Ordovician carbonate platforms

Upper Ordovician carbonate rocks are widespread around the world, including in Laurentia, peri-Gondwana, Siberia, Baltoscandia, and other micro-continents and terranes that mainly developed on palaeo-continental margins in tropical to sub-tropical regions (e.g., Read 1982; Webby 2002; Kiessling et al. 2003; James et al. 2020) (Table 2). In general, like the Xiazhen platform, these are ramp-type platforms that are composed of peritidal flats and inner to outer shallow subtidal facies, with local shoals and reefs as well as lagoons in the platform interior regardless of tectonic settings. Similarities between these platforms include (Table 2): (a) dominance of skeletal grains throughout the platform; (b) rarity of ooid shoals; and c) an absence of skeletal barrier reefs; in fact, Late Ordovician rimmed platforms were very much limited (Webby 2002, p. 160). These models correspond to the post-GOBE-type carbonate facies model, which is characterised by a decrease in ooids, microbialites, and flat-pebble conglomerates, together with an increase in skeletal grains, metazoan-skeletal reefs, and burrows (Droser and Bottjer 1989; Li and Droser 1997, 1999; Liu 2009; Pruss et al. 2010; Liu et al. 2011; Wright and Cherns 2016; Lee and Riding 2018).

The current study demonstrates that the overall depositional pattern of the Xiazhen Formation was generally similar to that of other Upper Ordovician ramp-type carbonate platforms around the world, and the formation provides a typical example of the Upper Ordovician (especially Katian) carbonate depositional model (Fig. 7; Table 2). The rarity of Late Ordovician rimmed platforms was at least partly caused by the absence of skeletal barrier reefs because early skeletal organisms constructed only small patch reefs during the Ordovician (Webby 2002). Rimmed platforms became more common in the Silurian and Devonian when barrier reef complexes of tabulate and rugose corals, stromatoporoids, bryozoans, algae, and calcimicrobes appeared (Bourque 1988; Soja 1991; Lavoie et al. 1992; de Freitas and Mayr 1998; Cooper 2002). The Late Ordovician was also characterised by global cooling and a decrease in pCO_2 (Trotter et al. 2008; Liu et al. 2020) associated with oxygenation of the shallow-marine environment (Lee and Riding 2018; Edwards 2019) prior to the Hirnantian glaciation event. These palaeoceanographic conditions could have decreased the carbonate saturation state (James et al. 2020), inducing the disappearance of ooids (e.g., Liu et al. 2011) as well as microbialites (Riding 2006; Lee and Riding 2018) in the later Ordovician. These changes would have coincided with the diversification of skeletal organisms that provided skeletal grains to Late Ordovician carbonate platforms (Li and Droser 1999; Pruss et al. 2010).

Conclusions

(1) The middle to upper Xiazhen Formation comprises eight depositional facies and twenty-four shallowing-upward depositional cycles, including mixed carbonate–clastic subtidal cycles, carbonate subtidal cycles, and peritidal-capped subtidal cycles. The reconstructed depositional models based on the vertical association of cyclic facies collectively indicate a ramp-type mixed siliciclastic–carbonate platform controlled by clastic sediment input and relative sea-level change.

(2) The carbonate platforms of the Xiazhen Formation would have developed during the Katian, prior to the Hirnantian glaciation event. Ramp-type carbonate platforms similar to the Xiazhen Formation mainly formed during the Late Ordovician, and are characterised by their grain composition (dominant skeletal grains with rare ooids) and reef types (absence of skeletal barrier reefs). It is suggested that the appearance of new skeletal organisms during the GOBE that were not yet capable of constructing barrier reefs as well as the accompanying palaeoceanographic conditions (e.g., global cooling, decrease in pCO_2, and shallow-marine oxygenation) may have been responsible for this appearance of Upper Ordovician-type carbonate platforms.

Acknowledgements We thank reviewer BR Pratt, an anonymous reviewer, and editor W Kiessling for their constructive comments and suggestions. We are also grateful to D-J Lee, D-C Lee, J Hong, and J Jeon for the identification of fossils and helpful comments on an earlier version of the manuscript.

Funding This study was supported by grants from the National Research Foundation of Korea to JP (2019R1I1A1A01061336), to JHL (2019R1A2C4069278), and to SJC (2018R1A2A2A05018469), and from the Chinese Academy of Sciences to KL (XDB26000000).

Availability of data and materials Not applicable.

Code availability Not applicable.

Compliance with ethical standards

Conflict of interest The authors declare that they have no conflict of interest.

References

Aigner T (1985) Storm depositional systems: dynamic stratigraphy in Modern and ancient shallow-marine sequences. Lecture Notes in Earth Sciences 3. Springer-Verlag, Berlin

Batten Hender KL, Dix GR (2006) Facies, geometry and geological significance of Late Ordovician (early Caradocian) coral bioherms: Lourdes Formation, western Newfoundland. Sedimentology 53:1361–1379

Batten Hender KL, Dix GR (2008) Facies development of a Late Ordovician mixed carbonate-siliciclastic ramp proximal to the developing Taconic orogen: Lourdes Formation, Newfoundland, Canada. Facies 54:121–149

Bourque P-A (1988) Silurian reefs. In: Geldsetzer HHJ, James NP, Tebbutt GE (eds) Reefs, Canada and adjacent areas. CSPG Special Publications-Memoir 13, pp 245–250

Bova JA, Read JF (1987) Incipiently drowned facies within a cyclic peritidal ramp sequence, Early Ordovician Chepultepec interval, Virginia Appalachians. Geol Soc Am Bull 98:714–727

Burchette TP, Wright VP (1992) Carbonate ramp depositional systems. Sed Geol 79:3–57

Carlucci JR, Westrop SR, Brett CE, Burkhalter R (2014) Facies architecture and sequence stratigraphy of the Ordovician Bromide Formation (Oklahoma): a new perspective on a mixed carbonate-siliciclastic ramp. Facies 60:987–1012

Chen J, Chough SK, Han Z, Lee J-H (2011) An extensive erosion surface of a strongly deformed limestone bed in the Gushan and Chaomidian formations (late Middle Cambrian to Furongian), Shandong Province, China: Sequence–stratigraphic implications. Sed Geol 233:129–149

Chen J, Lee J-H, Woo J (2014) Formative mechanisms, depositional processes, and geological implications of Furongian (late Cambrian) reefs in the North China Platform. Palaeogeogr Palaeoclimatol Palaeoecol 414:246–259

Chen Q, Fan J, Zhang L, Chen X (2018) Paleogeographic evolution of the Lower Yangtze region and the break of the "platform-slope-basin" pattern during the Late Ordovician. Science China Earth Sciences 61:625–636

Chen X, Rong J-Y, Qiu J-Y, Han N-R, Li L-Z, Li S-J (1987) Late Ordovician stratigraphy, sedimentology and environment of Zhuzhai of Yushan, Jiangxi. Journal of Stratigraphy 11:23–34 ((**In Chinese with English abstract**))

Chen Z-Y, Kim M-H, Choh S-J, Lee D-J, Chen X (2016) Discovery of *Anticostia uniformis* from the Xiazhen Formation at Zhuzhai, South China and its stratigraphic implication. Palaeoworld 25:356–361

Copper P (2002) Silurian and Devonian reefs: 80 million years of global greenhouse between two ice ages. In: Kiessling W, Flügel E, Golonka J (eds) Phanerozoic reef patterns. SEPM Special Publication, New York, pp 181–238

Dai M, Liu L, Lee D-J, Peng U, Miao A (2015) Morphometrics of *Heliolites* (Tabulata) from the Late Ordovician, Yushan, Jiangxi, South China. Acta Geol Sin 89:38–54

de Freitas T, Mayr U (1998) Upper Ordovician to Lower Devonian (Richmondian to Emsian carbonate platforms and the Boothia Uplift synorogenic succession. In: Mayr U, de Freitas T, Beauchamp N, Eisbacher G (eds) The geology of Devon Island north of

76°, Canadian Arctic Archipelago. Geological Survey of Canada Bulletin 526, pp 57–154
Demicco RV, Hardie LA (1994) Sedimentary structures and early diagenetic features of shallow marine carbonate deposits. SEPM Atlas Series No. 1, Tulsa, Oklahoma
Droser ML, Bottjer DJ (1989) Ordovician increase in extent and depth of bioturbation: Implications for understanding early Paleozoic ecospace utilization. Geology 17:850–852
Edwards CT (2019) Links between early Paleozoic oxygenation and the Great Ordovician Biodiversification Event (GOBE): a review. Palaeoworld 28:37–50
Fergusson CL (2009) Tectonic evolution of the Ordovician Macquarie Arc, central New South Wales: arguments for subduction polarity and anticlockwise rotation. Aust J Earth Sci 56:179–193
Flügel E (2004) Microfacies of carbonate rocks: analysis, interpretation and application. Springer, Berlin
Folk RL (1987) Detection on organic matter in thin-sections of carbonate rocks using a white card. Sed Geol 54:193–200
Gao D, Lin C, Yang H, Zuo F, Cai Z, Zhang L, Liu J, Li H (2014) Microfacies and depositional environments of the Late Ordovician Lianglitage Formation at the Tazhong Uplift in the Tarim Basin of Northwest China. J Asian Earth Sci 83:1–12
Gao Z, Fan T (2014) Intra-platform tectono-sedimentary response to geodynamic transition along the margin of the Tarim Basin, NW China. J Asian Earth Sci 96:178–193
Grimwood JL, Coniglio M, Armstrong DK (1999) Blackriveran carbonates from the subsurface of the Lake Simcoe area, southern Ontario: stratigraphy and sedimentology of a low-energy carbonate ramp. Can J Earth Sci 36:871–889
Harris MT, Sheehan PM, Ainsaar L, Hints L, Männik P, Nõlvak J, Rubel M (2004) Upper Ordovician sequences of western Estonia. Palaeogeogr Palaeoclimatol Palaeoecol 210:135–148
Holmden C, Creaser RA, Muehlenbachs K, Leslie SA, Bergström SM (2008) Isotopic evidence for geochemical decoupling between ancient epeiric seas and bordering oceans: implications for secular curves. Geology 26:567–570
Holland SM (1993) Sequence stratigraphy of a carbonate-clastic ramp: the Cincinnatian Series (Upper Ordovician) in its type area. Geol Soc Am Bull 105:306–322
Holland SM, Patzkowsky ME (2009) The stratigraphic distribution of fossils in a tropical carbonate succession: Ordovician Bighorn Dolomite, Wyoming, USA. Palaios 24:303–317
Holland SM, Patzkowsky ME (2012) Sequence architecture of the Bighorn Dolomite, Wyoming, USA: transition to the Late Ordovician icehouse. J Sediment Res 82:599–615
Husinec A (2016) Sequence stratigraphy of the Red River Formation, Williston Basin, USA: stratigraphic signature of the Ordovician Katian greenhouse to icehouse transition. Mar Pet Geol 77:487–506
James NP, Narbonne GM, Armstrong AKR (2020) Aragonite depositional facies in a Late Ordovician calcite sea, Eastern Laurentia. Sedimentology 67:3513–3532
Jeon J, Liang K, Lee M, Kershaw S (2020a) Earliest known spatial competition between stromatoporoids: evidence from the Upper Ordovician Xiazhen Formation of South China. J Paleontol 94:1–10
Jeon J, Liang K, Park J, Choh S-J, Lee D-J (2020b) Late Ordovician stromatoporoids from the Xiazhen Formation of South China: paleoecological and paleogeographical implications. Geol J 55:197–209
Jin J, Zhan R, Wu R (2018) Equatorial cold-water tongue in the Late Ordovician. Geology 46:759–762
Johnson RE, Sheehan PM (1985) Late Ordovician dasyclad algae of the eastern Great Basin. In: Toomey DF, Nitecki MH (eds) Paleoalgology: contemporary research and applications. Springer-Verlag, Berlin, Heidelberg, New York, Tokyo, pp 79–84
Kiessling W, Flügel E, Golonka J (2003) Patterns of phanerozoic carbonate platform sedimentation. Lethaia 36:195–226
Kröger B, Penny A, Shen Y, Munnecke A (2020) Algae, calcitarchs and the Late Ordovician Baltic limestone facies of the Baltic Bain. Facies 66:12. https://doi.org/10.1007/s10347-019-0585-0)
Kwon S-W, Park J, Choh S-J, Lee D-C, Lee D-J (2012) Tetradiid-siliceous sponge patch reefs from the Xiazhen Formation (late Katian), southeast China: a new Late Ordovician reef association. Sed Geol 267–268:15–24
Lavoie D, Bourque P-A, Héroux Y (1992) Early Silurian carbonate platforms in the Appalachian orogenic belt: The Sayabec—La Vieille formations of the Gaspé-Matapédia basin, Quebec. Can J Earth Sci 29:704–719
Lee D-C, Park J, Woo J, Kwon YK, Lee J-G, Guan L, Sun N, Lee S-B, Liang K, Liu L, Rhee C-W, Choh S-J, Kim B-S, Lee D-J (2012) Revised stratigraphy of the Xiazhen Formation (Upper Ordovician) at Zhuzhai, South China, based on palaeontological and lithological data. Alcheringa 36:387–404
Lee D-C (2013) Late Ordovician trilobites from the Xiazhen Formation in Zhuzhai, Jiangxi Province, China. Acta Palaeontol Pol 58:855–882
Lee M, Elias RJ, Choh S-J, Lee D-J (2016a) Insight from early coral-stromatoporoid intergrowth, Late Ordovician of China. Palaeogeogr Palaeoclimatol Palaeoecol 463:192–204
Lee M, Park H, Tien NV, Choh S-J, Elias R, Lee D-J (2016b) A new species of *Amsassia* from the Ordovician of Korea and South China: paleobiological and paleogeographical significance. Acta Geol Sin 90:796–806
Lee M, Elias RJ, Choh S-J, Lee D-J (2019a) Disorientation of corals in Late Ordovician lime mudstone: a case for ephemeral, biodegradable substrate? Palaeogeogr Palaeoclimatol Palaeoecol 520:55–65
Lee M, Elias RJ, Choh S-J, Lee D-J (2019b) Palaeobiological features of the coralomorph *Amsassia* from the Late Ordovician of South China. Alcheringa 43:18–32
Lee J-H, Chen J, Chough SK (2015) The middle–late Cambrian reef transition and related geological events: a review and new view. Earth Sci Rev 145:66–84
Lee J-H, Riding R (2018) Marine oxygenation, lithistid sponges, and the early history of Paleozoic skeletal reefs. Earth Sci Rev 181:98–121
Li Q, Li Y, Kiessling W (2015) Allogenic succession in Late Ordovician reefs from southeast China: a response to the Cathaysian orogeny. Estonian Journal of Earth Sciences 64:68–73
Li Q, Lehnert O, Wu R, Park J, Liang K, Yu S, Mao Y, Na Y (2020) The palaeokarst in the Xiazhen Formation (Late Ordovician): a record of the mid-Katian glaciation in South China. 2020 Virtual Annual Meeting of IGCP 653 - Zooming in on the GOBE, Denmark (online)
Li W, Chen J, Wang L, Fang X, Zhang Y (2019) Slump sheets as a record of regional tectonics and paleogeographic changes in South China. Sed Geol 392:105525
Li X, Droser ML (1997) Nature and distribution of Cambrian shell concentrations: Evidence from the Basin and Range Province of the Western United States (California, Nevada, and Utah). Palaios 12:111–126
Li X, Droser ML (1999) Lower and Middle Ordovician shell beds from the Basin and Range Province of the Western United States (California, Nevada, and Utah). Palaios 14:215–233
Li Y, Kershaw S, Mu X (2004) Ordovician reef systems and settings in South China before the Late Ordovician mass extinction. Palaeogeogr Palaeoclimatol Palaeoecol 205:235–254
Liang K, Elias RJ, Choh S-J, Lee D-C (2016) Morphometrics and paleoecology of *Catenipora* (Tabulata) from the Xiazhen Formation (Upper Ordovician), Zhuzhai, South China. J Paleontol 90:1027–1048

Liu J (2009) Marine sedimentary response to the Great Ordovician Biodiversification Event: examples from North China and South China. Paleontol Res 13:9–21

Liu J, Zhan R, Dai X, Liao H, Ezaki Y, Adachi N (2011) Demise of Early Ordovician oolites in South China: Evidence for paleoceanographic changes before the GOBE. In: Gutiérrez-Marco JC, Rábano I, García-Bellido D (eds) Ordovician of the World. Cuadernos del Museo Geominero 14, Instituto Geológico y Minero de España, Madrid, pp 309–317

Liu L, Liang L, Wu Y, Zhou X, Jia L, Riding R (2020) Ordovician cyanobacterial calcification: A marine fossil proxy for atmospheric CO_2. Earth Planet Sci Lett 530:115950

Loi A, Ghienne JF, Dabard MP, Paris F, Botquelen A, Christ N, Elaouad-Debbaj Z, Gorini A, Vidal M, Videt B, Destombes J (2010) The Late Ordovician glacio-eustatic record from a high-latitude storm-dominated shelf succession: The Bou Ingarf section (Anti-Atlas, Southern Morocco). Palaeogeogr Palaeoclimatol Palaeoecol 296:332–358

Macquaker JHS, Bentley SJ, Bohacs KM (2010) Wave-enhanced sediment-gravity flows and mud dispersal across continental shelves: reappraising sediment transport processes operating in ancient mudstone successions. Geology 38:947–950

Matthew AJ, Woods AJ, Oliver C (1991) Spots before the eyes: new comparison charts for visual percentage estimation in archaeological material. In: Middleton A, Freestone I (eds) Recent developments in ceramic petrology. British Museum Occasional Paper 81, British Museum, London, pp 211–264

McLaughlin PI, Brett CE, McLaughlin SLT, Cornell SR (2004) High-resolution sequence stratigraphy of a mixed carbonate-siliciclastic, cratonic ramp (Upper Ordovician; Kentucky—Ohio, USA): insight into the relative influence of eustasy and tectonics through analysis of facies gradients. Palaeogeogr Palaeoclimatol Palaeoecol 210:267–294

Nestor H, Webby BD (2013) Biogeography of the Ordovician and Silurian stromatoporoidea. In: Harper DAT, Servais T (eds) Early Palaeozoic biogeography and palaeogeography. Geological Society of London Memoir, London, pp 67–79

O'Brien NR, Brett CE, Taylor WL (1994) Microfabric and taphonomic analysis in determining sedimentary processes in marine mudstones: example from Silurian of New York. J Sediment Res 64:847–852

Osleger D (1991) Subtidal carbonate cycles: Implications for allocyclic vs. autocyclic controls. Geology 19:917–920

Park J, Lee J-H, Hong J, Choh S-J, Lee D-C, Lee D-J (2015) An Upper Ordovician sponge-bearing micritic limestone and implication for early Palaeozoic carbonate successions. Sed Geol 319:124–133

Park J, Hong J, Lee J-H, Choh S-J, Lee D-J (2017a) Early labechiid stromatoporoids of the Yeongheung Formation (Middle Ordovician), Yeongwol Group, mideastern Korean Peninsula: Part I. Environ Distrib Geosci J 21:317–329

Park J, Lee J-H, Hong J, Choh S-J, Lee D-C, Lee D-J (2017b) Crouching shells, hidden sponges: Unusual Late Ordovician cavities containing sponges. Sed Geol 347:1–9

Pope MC (2014) High-resolution sequence stratigraphy of the Upper Ordovician Montoya Group, southern New Mexico and western Texas: Outcrop analog of an unconventional chert and carbonate reservoir. AAPG Bull 98:1577–1597

Potter PE, Maynard JB, Depetris PJ (2005) Mud and mudstones: introduction and review. Springer, Berlin, Heidelberg, New York

Pratt BR (2010) Peritidal carbonates. In: James NP, Dalrymple RW (eds) Facies models 4. GEOText6, Geological Association of Canada, pp 401–420

Pratt BR, Haidl FM (2008) Microbial patch reefs in Upper Ordovician Red River strata, Williston Basin, Saskatchewan: signal of heating in a deteriorating epeiric sea. In: Pratt BR, Holmden C (eds) Dynamics of Epeiric Seas. Geological Association of Canada, Special Publication 48, pp 303–340

Pratt BR, Raviolo MM, Bordonaro OL (2012) Carbonate platform dominated by peloidal sands: Lower Ordovician La Silla Formation of the eastern Precordillera, San Juan, Argentina. Sedimentology 59:843–866

Pruss SB, Finnegan S, Fischer WW, Knoll AH (2010) Carbonate in skeleton-poor seas: new insight from Cambrian and Ordovician strata of Laurentia. Palaios 25:73–84

Read JF (1982) Carbonate platforms of passive (extensional) continental margins: types, characteristics and evolution. Tectonophysics 81:1995–2212

Riding R (2000) Microbial carbonates: the geological record of calcified bacterial–algal mats and biofilms. Sedimentology 47:179–214

Riding R (2006) Microbial carbonate abundance compared with fluctuations in metazoan diversity over geological time. Sed Geol 185:229–238

Rong J-Y, Chen X (1987) Faunal differentiation, biofacies and lithofacies patterns of the Late Ordovician (Ashgillian) in South China. Acta Palaeontologica Sinica 26:507–535 ((**In Chinese with English abstract**))

Schlager W (1989) Drowning unconformities on carbonate platforms. In: Crevello PD, Wilson JL, Sarg JF, Read JF (eds) Controls on carbonate platform and basin development. SEPM Special Publication 44, pp 15–25

Schlager W (1999) Type 3 sequence boundaries. In: Harris PM, Saller AH, Simo JA (eds) Advances in carbonate sequence stratigraphy: application to reservoirs, outcrops, and models. SEPM Special Publication 63, pp 35–46

Schieber J (2016) Mud re-distribution in epicontinental basins—exploring likely processes. Mar Pet Geol 71:119–133

Scotese CR, Wright N (2018) PALEOMAP Paleodigital Elevation Models (PaleoDEMS) for the Phanerozoic PALEOMAP Project. https://www.earthbyte.org/paleodem-resource-scotese-and-wright-2018/. Accessed 8 Jan 2021

Semeniuk V (1973) Nearshore to offshore facies and depositional history of the Ordovician Daylesford Limestone, New South Wales. J Geol Soc Aust 20:449–464

Soja CM (1991) Origin of Silurian reefs in the Alexander Terrane of Southeastern Alaska. Palaios 6:111–125

Su W (2007) Tectonic and eustatic control on the distribution of black-shale source beds in the Wufeng and Longmaxi formations (Ordovician–Silurian), South China. Front Earth Sci China 1:470–481

Sun N, Lee D, Wang X (2014a) Septal patterns in Agetolites from the Xiazhen Formation (Upper Ordovician) at Zhuzhai, Yushan County, Jiangxi Province, South China. Sci China Earth Sci 57:247–257

Sun N, Elias RJ, Lee D-J (2014b) The biological affinity of *Amsassia*: new evidence from the Ordovician of North China. Palaeontology 57:1067–1089

Sun N, Elias RJ, Choh S-J, Lee D-C, Wang X-L, Lee D-J (2016) Morphometrics and palaeoecology of the coral *Agetolites* from the Xiazhen Formation (Upper Ordovician), Zhuzhai, South China. Alcheringa 40:251–274

Sun N, Elias RJ, Lee D-J (2019) Corallite increase in the Late Ordovician coral Agetolites, and its taxonomic implication. J Paleontol 93:839–855

Torsvik TH, Cocks LRM (2017) Earth history and palaeogeography. Cambridge University Press, Cambridge

Trotter JA, Williams IS, Barnes CR, Lécuyer C, Nicoll RS (2008) Did cooling oceans trigger Ordovician Biodiversification? Evidence from conodont thermometry. Science 321:550–554

Webby BD (2002) Patterns of Ordovician reef development. In: Kiessling W, Flügel E, Golonka J (eds) Phanerozoic reef patterns, vol 72. SEPM Special Publication, London, pp 129–179

Webby BD (2004) Stromatoporoids. In: Webby BD, Paris F, Droser ML, Percival IG (eds) The great Ordovician biodiversification event. Columbia University Press, New York, pp 112–118

Webby BD, Paris F, Droser ML, Percival IG (2004) The great Ordovician biodiversification event. Columbia University Press, New York

Wright VP, Cherns L (2016) Leaving no stone unturned: the feedback between increased biotic diversity and early diagenesis during the Ordovician. J Geol Soc 173:241–244

Zhan R-B, Rong J-Y, Jin J, Cocks LRM (2002) Late Ordovician brachiopod communities of southeast China. Can J Earth Sci 39:445–468

Zhang F (2016) Recognizing morphospecies in the heliolitid coral Plasmoporella. Palaeoworld 25:32–42

Zhang M, Xia F-S, Taylor PD, Liang K, Ma J-Y (2018) Upper Ordovician bryozoans from the Xiazhen Formation of Yushan, northeastern Jiangxi, East China. Palaeoworld 27:343–359

Zhang Y, Chen X, Yu G, Goldman D, Liu X (2007) Ordovician and Silurian rocks of northwest Zhejiang and northeast Jiangxi provinces. University of Science and Technology of China Press, Hefei, SE China